Dispersion Properties of Micropolar Plates Through the Partial Wave Technique

ANNAMARIA PAU and MARCO LEPIDI

ABSTRACT

The focus of this study is on the dynamic problem of free guided propagation of harmonic elastic waves in homogeneous plates modeled as a linear micropolar continuum, in the absence of dissipation. The plate is modeled as an infinite layer with finite thickness, bounded by two parallel traction-free planes. The analysis is carried out using the analytical partial wave technique, which returns the dispersion relation in terms of wavenumber as a function of frequency, as well as the wavemode shapes. The dispersion relation for the micropolar continuum differs markedly from that of a Cauchy continuum, above all for the presence of microrotation modes – unique to the Cosserat continuum. Morphological modification of the standing wavemodes, as well as the occurrence of internal resonance conditions and inter-wave transfer of mechanical energy, are observed among microrotation waveforms and other waveforms.

INTRODUCTION

In a micropolar continuum, each material point possesses six independent degrees of freedom: three translations and three rotations. In accordance with the mechanical principle of duality, adjacent infinitesimal volumes interact by independent contact forces and couples. The early formulation of this mechanical model is attributed to the Cosserat brothers and dates back to the beginning of the past century [1]. Initially, micropolar models were developed to describe the behavior of granular media and particulate matter. Over time, their use has extended to crystalline solids, fiber-reinforced materials, composites, and architected metamaterials, whose microstructural effects can be captured at the macroscale by equivalent homogenization [2]. In wave propagation problems with small-scale effects, micropolar models become essential, particularly when wavelengths are comparable to internal length scales [3]. Since the 1960s, eminent scientists have laid the foundation for bulk wave propagation in micropolar media [4–7], highlighting unique dynamic phenomena such as cutoff frequencies and novel wave types [8].

Annamaria Pau, Associate Professor, Email: annamaria.pau@uniroma1.it Department of Structural and Geotechnical Engineering, Sapienza University of Rome, Rome, Italy
Marco Lepidi, Associate Professor, Email: marco.lepidi@unige.it Department of Civil, Chemical and Environmental Engineering, University of Genoa, Genoa, Italy

This study builds on that background to investigate harmonic wave propagation in a finite-thickness isotropic micropolar plate. The work emphasizes the role of microstructural parameters in wave behavior and aims to fill the gaps left by previous investigations [9–11], which lacked complete wavemode analyzes. Compared with classical Cauchy continua, micropolar plates exhibit a richer dispersion behavior. New spectral branches related to pure microrotation arise, along with complex interactions between wave modes. Methodologically, the present study moves beyond the technique of potentials, by recurring to the partial wave technique for better generality in deriving the dispersion relations and wavemodes. The objectives are to analyze dispersion curves, characterize new branches, and describe resonance effects. Internal resonances and modal interactions can lead to energy transfer across wave types. Identifying these regions is key to both theoretical insight and experimental observation of micropolar effects.

EQUATIONS OF MOTION OF MICROPOLAR CONTINUA

The model of the micropolar continuum is based on the linear theory of micropolar elasticity proposed by Eringen [8]. The set of coupled differential equations that govern the free undamped motion of an isotropic micropolar continuum are

$$\begin{aligned}(\mu+\kappa)\Delta\mathbf{u}+(\lambda+\mu)\nabla(\operatorname{div}\mathbf{u})+\kappa\operatorname{curl}\boldsymbol{\theta}&=\rho\ddot{\mathbf{u}}\\ \gamma\Delta\boldsymbol{\theta}+(\alpha+\beta)\nabla(\operatorname{div}\boldsymbol{\theta})+\kappa\operatorname{curl}\mathbf{u}-2\kappa\boldsymbol{\theta}&=\rho J\ddot{\boldsymbol{\theta}}\end{aligned} \tag{1}$$

where $\mathbf{u}$ and $\boldsymbol{\theta}$ are, respectively, the unknown displacement and microrotation vector fields that are a function of time t and of the position vector $\mathbf{x}=(x_1,x_2,x_3)^\top$. The double dots indicate second derivative with respect to time t. Moreover, $\lambda,\mu,\alpha,\beta,\gamma$ and κ are material moduli, ρ is the density of the material, and ρJ is the rotational inertia. The differential operators, when applied to a vector field $\mathbf{v}=(v_1,v_2,v_3)^\top$ indicate the operations $\Delta\mathbf{v}_i=v_{i,i}+v_{i,j}+v_{i,k}$, $\operatorname{div}\mathbf{v}=v_{1,1}+v_{2,2}+v_{3,3}$, $\operatorname{curl}\mathbf{v}_i=(-1)^{(i-1)}(v_{k,j}-v_{j,k})$ where the comma subscript indicates derivation with respect to the spatial coordinates, while the indices $i=1,2,3, j=1,2,3$ and $k=1,2,3$. The gradient ∇ applied to a scalar field ϕ gives the vector $\nabla\phi=(\phi_{,1}\ \phi_{,2}\ \phi_{,3})^\top$.

The homogeneous linear equations of motion (1) admit solutions in the class of plane waves oscillating harmonically in time with real-valued frequency ω while propagating periodically in space along the direction of the versor $\mathbf{n}=(n_1,n_2,n_3)^\top$ with wavevector $\mathbf{k}=k\mathbf{n}=(k_1,k_2,k_3)^\top$. Progressive waves advancing the positive $\mathbf{n}$-direction are

$$\mathbf{u}(\mathbf{x},t)=\mathbf{a}\,\mathrm{e}^{I(\mathbf{k}\cdot\mathbf{x}-\omega t)}+cc,\quad \boldsymbol{\theta}(\mathbf{x},t)=\mathbf{b}\,\mathrm{e}^{I(\mathbf{k}\cdot\mathbf{x}-\omega t)}+cc \tag{2}$$

where $\mathbf{a}$ and $\mathbf{b}$ are complex amplitude vectors, I is the imaginary unit and cc stands for complex conjugate. Substitution of the tentative solution (2) into equations (1) leads to the algebraic eigenproblem

$$\begin{aligned}k^2[(\lambda+2\mu+\kappa)\mathbf{L}\mathbf{a}+(\mu+\kappa)(\mathbf{I}-\mathbf{L})\mathbf{a}-I\kappa/k(\mathbf{n}\times\mathbf{b})]&=\rho\,\omega^2\mathbf{a}\\ k^2[(\alpha+\beta+\gamma+2\kappa/k^2)\mathbf{L}\mathbf{b}+(\gamma+2\kappa/k^2)(\mathbf{I}-\mathbf{L})\mathbf{b}-I\kappa/k(\mathbf{n}\times\mathbf{a})]&=\rho\,J\omega^2\mathbf{b},\end{aligned} \tag{3}$$

where $\mathbf{L}=\mathbf{n}\otimes\mathbf{n}$ and the symbol $\otimes$ stands for tensor product. Variables ω^2 and $\boldsymbol{\varphi}=(\boldsymbol{\varphi}_a,\boldsymbol{\varphi}_b)$ play the role of unknown eigenvalue and eigenvector, respectively. The eigensolution consists of six eigenpairs $(\omega^2,\boldsymbol{\varphi})$. Subproblems related to in-plane (x_1,x_3) and out-of-plane (x_1,x_2) vibrations turn out to be decoupled.

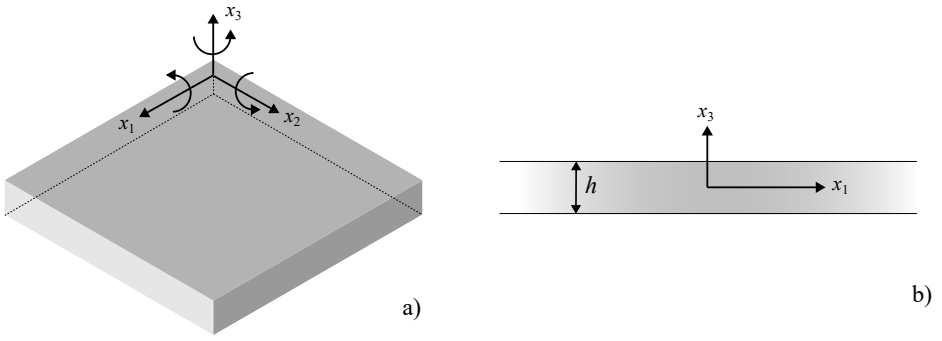

Figure 1. Micropolar plate: (a) sketch and reference system, (b) cross-section in plane (x_1, x_3).

GUIDED WAVE PROPAGATION IN MICROPOLAR PLATES

Analyses are focused on the in-plane vibrations of a *micropolar plate*, which is intended as a finite-thickness layer extracted from an infinite three-dimensional Cosserat continuum confined between two parallel planes (Figure 1a). The origin of the Cartesian system is placed on the mid-plane $\mathcal{M}$, identified by vectors $\mathbf{e}_1$ and $\mathbf{e}_2$ and spanned by coordinates x_1 and x_2. Consequently, the $\mathcal{M}$-orthogonal vector $\mathbf{e}_3$ is oriented along the finite thickness of the plate, denoted as height h and spanned by the coordinate x_3 (Figure 1b). The $\mathbf{e}_3$-orthogonal parallel planes play the role of *upper* $(x_3 = h/2)$ and *lower* $(x_3 = -h/2)$ free surfaces. The wave propagation is governed by the equations of motion (1), equipped with free-stress and free-couple-stress boundary conditions, reading

$$\sigma_{33} = 0, \quad \sigma_{13} = 0, \quad m_{23} = 0, \qquad \text{on} \quad x_3 = \pm h/2 \tag{4}$$

where σ_{33}, σ_{13} are, respectively, the normal and tangent stress components acting on the external surfaces, and m_{23} is the microcouple inducing rotation about the axis x_2.

According to the partial wave technique [12, 13], guided waves are expressed as the product between (i) a function defined across the thickness of the plate (the standing wavemode), and (ii) a term that describes spatially-periodic propagation along the plane of the plate. This applies to both displacement and microrotation fields, which read

$$\mathbf{u}(\mathbf{x}_c, \mathbf{k}_c, \omega, t) = \tilde{\mathbf{u}}\, \mathrm{e}^{I(\mathbf{k}_c \cdot \mathbf{x}_c - \omega t)}, \qquad \boldsymbol{\theta}(\mathbf{x}_c, \mathbf{k}_c, \omega, t) = \tilde{\boldsymbol{\theta}}\, \mathrm{e}^{I(\mathbf{k}_c \cdot \mathbf{x}_c - \omega t)} \tag{5}$$

where $\tilde{\mathbf{u}} = (\tilde{u}_1, \tilde{u}_2, \tilde{u}_3)^\top$ and $\tilde{\boldsymbol{\theta}} = (\tilde{\theta}_1, \tilde{\theta}_2, \tilde{\theta}_3)^\top$ are the amplitude vectors. Tentative solutions (5) describe a progressive displacement-microrotation wave that harmonically oscillates in time with frequency ω while periodically propagating in the space spanned by coordinate vector $\mathbf{x}_c = (x_1, 0, x_3)^\top$ along the direction of wavevector $\mathbf{k}_c = (k_1, 0, k_3)^\top$. During propagation, the wave is reflected back and forth between the upper and lower surfaces, as long as the inclination angle $\chi = \arctan(k_3/k_1)$ differs from zero. Consequently, the propagation function – the waveform – can be re-parameterized as

$$\mathbf{u}(\mathbf{x}_c, k_1, \phi, \omega, t) = \tilde{\mathbf{u}}\, \mathrm{e}^{I(k_1(x_1 + \phi x_3) - \omega t)}, \quad \boldsymbol{\theta}(\mathbf{x}_c, k_1, \phi, \omega, t) = \tilde{\boldsymbol{\theta}}\, \mathrm{e}^{I(k_1(x_1 + \phi x_3) - \omega t)} \tag{6}$$

where the wavenumber k_3 is expressed as a function of k_1 and the inclination parameter $\phi = k_3/k_1 = \tan\chi$. By substituting the tentative solution (6) into the homogeneous equations of motion (1) a first algebraic eigenproblem $(\mathbf{K}(\phi, k_1) - \omega^2 \mathbf{M})\tilde{\mathbf{u}} = \mathbf{0}$ is obtained, where the inclination parameter ϕ is the primary unknown. The in-plane problem

in the field $\mathbf{p} = (u_1, u_3, \theta_2)^\top$ is considered, since it can be decoupled from the out-of-plane problem in the field $\mathbf{q} = (u_2, \theta_1, \theta_3)^\top$. Considering the frequency and wavenumber as a parameter pair $\boldsymbol{\lambda} = (\omega, k_1)$, a parametric sub-eigenproblem $\mathbf{P}(\phi, \boldsymbol{\lambda})\tilde{\mathbf{p}} = \mathbf{0}$ is defined, where ϕ plays the role of eigenvalue. For each parameter pair $\boldsymbol{\lambda}$ the characteristic equation provides three values of the unknown $\phi^2(\boldsymbol{\lambda})$. Each solution $\phi_j^2(\boldsymbol{\lambda})$ returns two eigenvalues $\phi_j^+(\boldsymbol{\lambda})$ and $\phi_j^-(\boldsymbol{\lambda})$ and two eigenvectors $\boldsymbol{\varphi}_j^+(\boldsymbol{\lambda})$ and $\boldsymbol{\varphi}_j^-(\boldsymbol{\lambda})$, with $j = 1, ..., 3$.

Due to the completeness of the eigenspace, the guided harmonic waves propagating along the plate can be expressed by linear superposition of all the eigenvectors. For the in-plane problem, the superposition reads

$$u_1 = \sum_{j=1}^{3} \mathrm{e}^{I\left[k_1(x_1+\phi_j^+(\boldsymbol{\lambda})x_3)-\omega t\right]} \varphi_{j1}^+(\boldsymbol{\lambda}) c_j^+ + \sum_{j=1}^{3} \mathrm{e}^{I\left[k_1(x_1+\phi_j^-(\boldsymbol{\lambda})x_3)-\omega t\right]} \varphi_{j1}^-(\boldsymbol{\lambda}) c_j^- \quad (7)$$

for longitudinal waves, and

$$u_3 = \sum_{j=1}^{3} \mathrm{e}^{I\left[k_1(x_1+\phi_j^+(\boldsymbol{\lambda})x_3)-\omega t\right]} \varphi_{j2}^+(\boldsymbol{\lambda}) c_j^+ + \sum_{j=1}^{3} \mathrm{e}^{I\left[k_1(x_1+\phi_j^-(\boldsymbol{\lambda})x_3)-\omega t\right]} \varphi_{j2}^-(\boldsymbol{\lambda}) c_j^- \quad (8)$$

$$\theta_2 = \sum_{j=1}^{3} \mathrm{e}^{I\left[k_1(x_1+\phi_j^+(\boldsymbol{\lambda})x_3)-\omega t\right]} \varphi_{j3}^+(\boldsymbol{\lambda}) c_j^+ + \sum_{j=1}^{3} \mathrm{e}^{I\left[k_1(x_1+\phi_j^-(\boldsymbol{\lambda})x_3)-\omega t\right]} \varphi_{j3}^-(\boldsymbol{\lambda}) c_j^- \quad (9)$$

for shear/microrotation waves. Once the state of stress and microcouple stress associated to the fields (7)-(9) is known for the generic position vector $\mathbf{x}_c = (x_1, 0, x_3)^\top$ of the plate, the boundary conditions (4) can be enforced. This procedure originates a second algebraic eigenproblem $\mathbf{C}_p(\omega, k_1)\mathbf{c}_p = \mathbf{0}$, where $\mathbf{c}_p = (c_1^+, c_2^+, c_3^+, c_1^-, c_2^-, c_3^-)^\top$. Indeed, the inverse dispersion relation $\omega(k_1)$ (or the direct dispersion relation $k_1(\omega)$) can be determined by assigning the real-valued wavenumber k_1 as free parameter and the real-valued frequency ω as unknown eigenvalue (or viceversa). Each eigenvalue $\omega_i(k_1)$ corresponds to an eigenvector $\mathbf{c}_i(k_1) = (c_{i1}^+, c_{i2}^+, c_{i3}^+, c_{i1}^-, c_{i2}^-, c_{i3}^-)^\top$ and specifies the i-th parameter pair $\boldsymbol{\lambda}_i = (\omega_i(k_1), k_1)$. The corresponding monoharmonic wave has the form $\mathbf{p}_i(\mathbf{x}_c, k_1, t) = p_i\, \mathrm{e}^{I(k_1 x_1 - \omega_i(k_1)t)}\, \boldsymbol{\psi}_i(k_1, x_3)$, where the standing ($x_1$-independent) part

$$\boldsymbol{\psi}_i(k_1, x_3) = \sum_{j=1}^{3} \mathrm{e}^{I\phi_j^+(\boldsymbol{\lambda}_i)x_3}\, \boldsymbol{\varphi}_j^+(\boldsymbol{\lambda}_i) c_{ij}^+ + \sum_{j=1}^{3} \mathrm{e}^{I\phi_j^-(\boldsymbol{\lambda}_i)x_3}\, \boldsymbol{\varphi}_j^-(\boldsymbol{\lambda}_i) c_{ij}^- \quad (10)$$

is referred to as *wavemode*, in analogy to standing waves (or modes).

DISPERSION RELATION AND INTERNAL RESONANCES

Since the dispersion relation $\omega(k_1)$ is generally multi-valued, the dispersion diagram is multi-branched, with different branches corresponding to distinct dispersion curves. The complete set of solutions is referred to as the dispersion spectrum. The dispersion diagrams for the micropolar plate characterized by thickness $h_\circ = 5 * 10^{-3}$ m and the particular set of constitutive parameters ($\alpha_\circ = \beta_\circ = \gamma_\circ = 168 * 10^4$ N, $\kappa_\circ = 51 * 10^4$ N/m^2, $\lambda_\circ = 549 * 10^8$ N/m^2, $\mu_\circ = 265 * 10^8$ N/m^2, $\rho_\circ = 2810$ kg/m^3, $J_\circ = 235 * 10^{-7}$ m^4/m^2) are considered. This parameter set corresponds to the higher level of constitutive coupling κ considered in a companion study [14]. The dispersion branches of the ten frequencies associated with the lowest phase speeds are reported in Figure 2. In the investigated range, a high density of dispersion branches is observed, also pointing out the dispersive nature of the micropolar continuum for guided waves. The majority of dispersion curves show cutoff frequencies, corresponding to the lowest attainable real values of ω. The

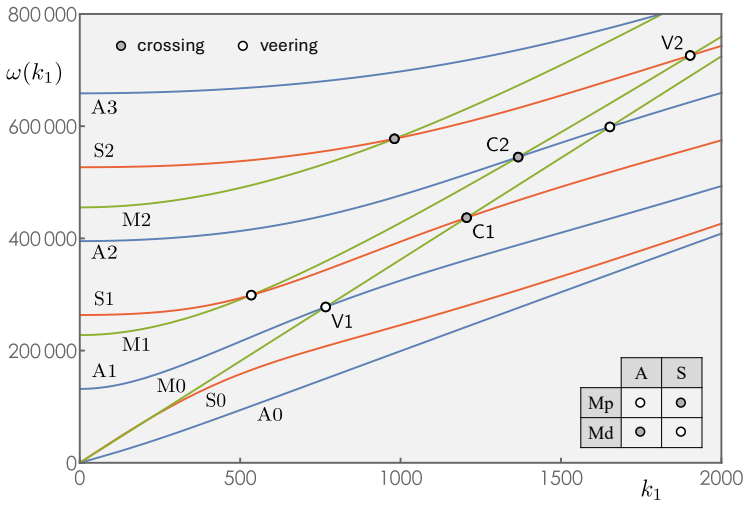

Figure 2. Dispersion diagram of in-plane guided waves propagating in the micropolar plate with classification of crossing and veering phenomena with $\omega(k_1)$ in [rad s^{-1}] and k_1 in [rad m^{-1}].

curve intersections in the dispersion diagram correspond to pairs of identical frequencies (for the same wavenumber), giving rise to *resonance* or *quasi-resonance* conditions.

By adopting the classical codification of Rayleigh-Lamb waves, the S-family of dispersion curves corresponds to *Symmetric waves* (red curves) and the A-family of dispersion curves corresponds to *Antisymmetric waves* (blue curves). The geometric criterion for classification depends on the morphology of the wavemode that characterizes each curve. Wavemodes A and S are dominated by the modal displacements υ_1 and υ_3, while negligibly participated by the microrotation ϑ_2. Symmetry and antisymmetry refer to the $\mathbf{k}_1$-aligned modal function $\upsilon_1(x_3)$ in the domain $\mathcal{X}_3 = \{x_3 : -h/2 \leq x_3 \leq h/2\}$.

As a peculiar consequence of micropolarity, a third family of dispersion curves must be introduced, which is not encountered in classical Cauchy plates. In fact, extra dispersion branches can be observed that correspond to wavemodes dominated by modal microrotation ϑ_2, while negligibly participated by the modal displacements υ_1 and υ_3. We denote by M-family this group of *microrotational waves* (green curves). Even-numbered waves M0, M2,... differ from odd-numbered waves M1, M3,... for the symmetric and antisymmetric structure of the dominant modal function $\vartheta_2(x_3)$ in the domain $\mathcal{X}_3$.

Resonance or nearly resonance conditions may respectively occur in the dispersion spectrum if the eigenvalue problem has a double solution $\omega_i(k_1)$ or a pair of close solutions $\omega_i(k_1)$ and $\omega_j(k_1)$ for a particular wavenumber k_1. This mathematical condition corresponds to the intersection or quasi-intersection of two different branches of the dispersion diagram. The mutual interplay among the two approaching eigenvalue loci can result in an intersection of the loci curves (*crossing* or *crossover phenomenon*) or in their sudden repulsion, when they veer away from each other with high and opposite curvatures (*avoided crossing* or *veering phenomenon*). Morphologically, the strong local interaction causes the eigenfunctions associated with the veering eigenvalues to interchange their morphologies in a rapid but continuous way (*hybridization phenomenon*).

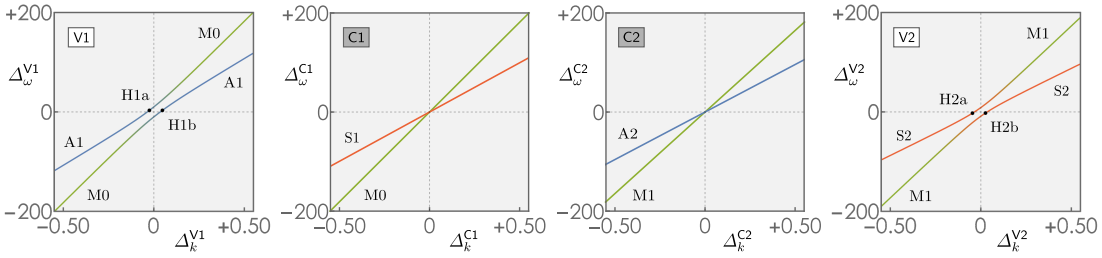

Figure 3. Resonance and nearly-resonance regions in the dispersion diagram.

Also, from the physical viewpoint, crossings and veerings open the possibility for significant energy exchanges between the associated resonant or quasi-resonant eigenfunctions. The mechanical system under investigation falls into the large class of mechanical systems in which veering phenomena occur as a consequence of the linear interaction between symmetric and antisymmetric modes [15–18].

From a mechanical perspective, intersections between two branches of the dispersion diagram of micropolar plates occur due to strong differences in the phase speeds of *slower* A and S waves and *faster* M waves. Several resonance conditions were identified (circles in Figure 2). Local analyses in the resonant regions enable to distinguish crossing phenomena (gray-filled circles) from veering phenomena (white-filled circles). A strong veering phenomenon, that does not happen for lower value of the constitutive coupling κ [14], occurs in the low-frequency range between waves M1 and S1. Four crossing and/or veering phenomena are selected to analyze the k_1-dependent evolution of the resonant wavemodes. Windows of the dispersion diagram centered at the crossings C1 and C2 and veerings V1 and V2 are shown in Figure 3, where $\Delta^{\mathsf{J}}_{\omega} = \omega - \omega_{\mathsf{J}}$ and $\Delta^{\mathsf{J}}_{k} = k_1 - k_{\mathsf{J}}$ with $\mathsf{J} = \mathsf{C1}, \mathsf{C2}, \mathsf{V1}, \mathsf{V2}$. The pairs of polarized wavemodes at crossings C1 and C2, and pairs of hybrid wavemodes at veerings V1 and V2 are reported in Figure 4.

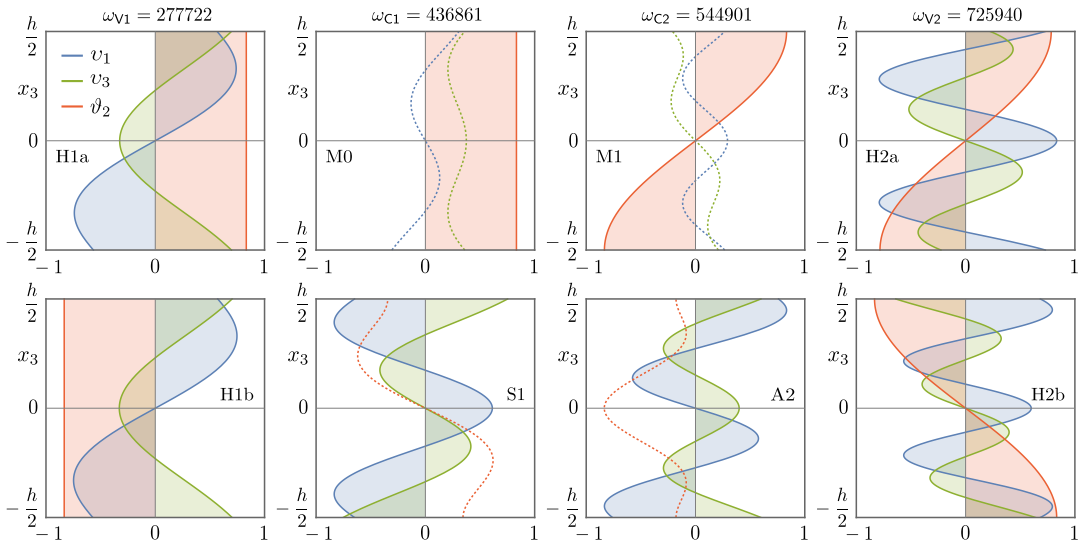

Figure 4. Polarized wavemodes at crossing points C1 and C2 and hybrid wavemodes at veerings V1 and V2. Dashing indicates small modal functions (shown with multiplicator $M = 2000$).

Perfectly resonant wavemodes at crossings C1 and C2 do not interact across the intersection of their dispersion curves. Consequently, they maintain unchanged their respective modal structures, characterized by strong displacement polarization (waves S1 and A2) and microrotation polarization (waves M0 and M1). Similar considerations are valid for the structures and polarizations of all the other pairs of symmetric or antisymmetic wavemodes involved in crossing phenomena.

Differently, the pairs of quasi resonant wavemodes at veerings V1 and V2 strongly interact with each other. In fact, the two veering wavemodes undergo a complete hybridization process, consisting of a progressive swap of their respective morphologies, until the exchange of the modal functions is completed. Since the process develops continuously, the two veering waves assume every possible degree of hybridization in the narrow region of quasi-resonance, reaching the highest level of hybridization at the minimal distance between the dispersion curves [19, 20]. As a paradigmatic example, the higher-frequency wave A1 (blue curve) and lower-frequency wave M0 (green curve) enter the veering region V1 (Figure 3) with strong displacement polarization and microrotation polarization, respectively. As their respective dispersion curves approach each other, the wavemodes start hybridizing (blended color curves), until the maximum hybridization corresponding to the minimum inter-curve distance is reached. The structures of hybrid wavemodes H1a and H1b at maximal hybridization show the same modal functions $\upsilon_1(x_3)$ and $\upsilon_3(x_3)$ combined with identical but opposite-signed modal function $\vartheta_2(x_3)$. Beyond the zone of maximum hybridization, the wavemodes complete the swap of their respective morphologies and leave the veering zone as lower-frequency wave A1 and higher-frequency wave M0 (exchanged polarizations). The same considerations can be extended to the structures and polarizations of the hybrid wavemodes H2a and H2b at veering V2 and all other pairs of hybrid modes involved in veering phenomena.

CONCLUDING REMARKS

The dispersion behavior of guided elastic waves in homogeneous micropolar plates has been investigated, by leveraging the partial wave technique to derive both the dispersion relations and associated wavemodes. The enriched kinematic framework including micropolarity determines higher spectral density in the dispersion diagram, by virtue of additional waves polarized in the microrotational degrees-of-freedom. Special focus has been placed on resonance and near-resonance conditions, manifested as crossing and veering phenomena of the dispersion branches. In particular, veering branches have been shown to undergo modal hybridization, with a continuous and complete exchange of the wavemodal structures across the resonance region. While similar effects may occur also in classical Cauchy continua, their existence has not been thoroughly explored. From a practical perspective, the occurrence and characteristics of veering phenomena are strongly influenced by the micropolar constitutive parameters, suggesting a potential route for their experimental identification through dispersion-based measurements. The present findings contribute to a deeper understanding of wave propagation in microstructured media and motivate further studies on the role of microstructure in modal interactions, both in generalized continuum models and in their classical counterparts.

ACKNOWLEDGMENT

Annamaria Pau gratefully acknowledges the financial support by Sapienza University with grant RD12318AAD49FEC0.

REFERENCES

1. Cosserat, E. and F. Cosserat. 1909. *Théorie des corps déformables*, A. Hermann et fils.
2. Gambarotta, L., A. Bacigalupo, and M. Lepidi. 2022. "Homogenization of periodic architected materials," in *50+ Years of AIMETA: A Journey Through Theoretical and Applied Mechanics in Italy*, Springer, pp. 399–417.
3. Pau, A. and P. Trovalusci. 2012. "Block masonry as equivalent micropolar continua: The role of relative rotations," *Acta Mechanica*, 223(7):1455 – 1471.
4. Truesdell, C. and R. A. Toupin. 1960. "The classical field theories," in S. Flügge, ed., *Encycolpedia of Physics*, Springer, Berlin, vol. III/2.
5. Mindlin, R. and H. Tiersten. 1962. "Effects of couple-stresses in linear elasticity," *Archive for Rational Mechanics and Analysis*, 11(1):415 – 448.
6. Pal'mov, V. 1964. "Fundamental equations of the theory of asymmetric elasticity," *Journal of Applied Mathematics and Mechanics*, 28(3):496 – 505.
7. Eringen, A. C. 1966. "Linear theory of micropolar elasticity," *Journal of Mathematics and Mechanics*, 15(6):909–923.
8. Parfitt, V. R. and A. C. Eringen. 1969. "Reflection of plane waves from the flat boundary of a micropolar elastic half-space," *Journal of the Acoustical Society of America*, 45:1258–1272.
9. Gauthier, R. and W. Jahsman. 1981. "A quest for micropolar elastic constants," *Archives of Mechanics*, 33(5):717 – 737.
10. Eringen, C. 1999. *Microcontinuum field theories I: Foundations and Solids*, Springer.
11. Kulseh, M., V. Matveenko, and I. Shardakov. 2007. "Constructing an analytical solution for lamb waves using the Cosserat continuum approach," *Journal of Applied Mechanics and Technical Physics*, 48(1):119 – 125.
12. Rose, J. L. 2014. *Ultrasonic guided waves in solid media*, Cambridge university press.
13. Pau, A. and F. Lanza Di Scalea. 2015. "Nonlinear guided wave propagation in prestressed plates," *Journal of the Acoustical Society of America*, 137(3):1529 – 1540.
14. Pau, A. and M. Lepidi. 2025. "Dispersion properties of guided elastic waves in micropolar plates," *Submitted*.
15. Triantafyllou, M. and G. Triantafyllou. 1991. "Frequency coalescence and mode localization phenomena: a geometric theory," *Journal of Sound and Vibration*, 150(3):485–500.
16. Vidoli, S. and F. Vestroni. 2004. "Veering phenomena in systems with gyroscopic coupling," *ASME Journal of Applied Mechanics*, 72(5):641–647.
17. Lepidi, M. and V. Gattulli. 2014. "A parametric multi-body section model for modal interactions of cable-supported bridges," *Journal of Sound and Vibration*, 333(19):4579–4596.
18. Gattulli, V., M. Lepidi, F. Potenza, and U. Di Sabatino. 2019. "Modal interactions in the nonlinear dynamics of a beam–cable–beam," *Nonlinear Dynamics*, 96(4):2547–2566.
19. du Bois, J. L., S. Adhikari, and N. A. J. Lieven. 2011. "On the quantification of eigenvalue curve veering: a veering index," *ASME Journal of Applied Mechanics*, 78(4):041007.
20. Lepidi, M. 2013. "Multi-parameter perturbation methods for the eigensolution sensitivity analysis of nearly-resonant non-defective multi-degree-of-freedom systems," *Journal of Sound and Vibration*, 332(4):1011–1032.